Mineralogical Magazine (2022), **86**, 346–353
doi:10.1180/mgm.2022.27

CAMBRIDGE UNIVERSITY PRESS

Article

Guite, the spinel-structured $Co^{2+}Co_2^{3+}O_4$, a new mineral from the Sicomines copper–cobalt mine, Democratic Republic of Congo

Zhilan Lei[1], Xinghai Chen[2], Jianxiong Wang[1]*, Yingchun Huang[1], Fangfang Du[1] and Zier Yan[3]

[1]Hunan Research Institute of Nonferrous Metals, #99 Yada Road, Zhanggongling, Changsha City, Hunan Province 410100, People's Republic of China; [2]La Sino-Congolaise Compagnie des Mines S.A., Quartier KAPATA, Commune DILALA, Ville de Kolwezi, Province de Lualaba, Democratic Republic of Congo; and [3]Rigaku Beijing Corporation, 2601A, Tengda Plaza, No. 168, Xizhimenwai Avenue, Haidian District, Beijing 100044, People's Republic of China

Abstract

Guite (IMA2017-080), Co_3O_4, is a new mineral species and an important economic mineral found in the Sicomines copper-cobalt mine, located ~11 km southwest of Kolwezi City, Democratic Republic of Congo. The mineral occurs as a granular agglomerate, 50 to 500 μm in size, and is associated closely with heterogenite in a quartz matrix. Guite is opaque, has a dark grey colour with metallic lustre and a black streak. In reflected light microscopy, it is white with no internal reflections. The reflectance values (in air, *R* in %) are: 27.0 (470 nm); 25.6 (546 nm); 25.2 (589 nm), and 24.6 (650 nm). The average of 20 electron-microprobe analyses is Co 71.53, Cu 0.58, Mn 0.67, Si 0.25, O 26.78, total 99.82 wt.%, corresponding to the empirical formula calculated on the basis of 4 O apfu: $(Co^{2+}_{0.92}Cu^{2+}_{0.02}Si^{4+}_{0.02})_{\Sigma 0.96}(Co^{3+}_{1.98}Mn^{3+}_{0.03})_{\Sigma 2.01}O_{4.00}$, with Co^{2+} and Co^{3+} partitioned using charge balance. The ideal formula is $Co^{2+}Co_2^{3+}O_4$. Guite is cubic with space group $Fd\bar{3}m$. The unit cell parameters refined from the single crystal X-ray diffraction data are: $a = 8.0898(1)$ Å, $V = 529.436(11)$ Å^3 and $Z = 8$. The calculated density of guite is 6.003 g/cm^3. The eight strongest observed powder X-ray diffraction lines [*d* in Å (*I*/*I*0) (*hkl*)] are: 4.6714 (16.7) (111), 2.8620 (18.4) (220), 2.4399 (100) (311), 2.3348 (10.4) (222), 2.0230 (24.8) (400), 1.5556 (26.3) (511, 333), 1.4296 (37.7) (440) and 1.0524 (10.1) (731, 553). The crystal structure of guite was determined by single-crystal X-ray diffraction and refined to $R = 0.0132$ for 3748 (69 unique) reflections. Guite has a typical spinel-type structure with Co^{2+} in tetrahedral coordination with a Co^{2+}–O bonding length of 1.941(1) Å, and Co^{3+} in octahedral coordination with a Co^{3+}–O bonding length of 1.919(1) Å. The structure is composed of cross-linked framework of chains of Co^{3+}–O_6 octahedra sharing the equilateral triangle edges (2.550 Å) in three directions [0 1 1], [1 1 0], [1 0 1] with Co^{2+} filling the tetrahedral interstices among the chains. Guite is named in honour of Prof. Xiangping Gu (1964–).

Keywords: guite, new mineral, Co_3O_4, Sicomines copper–cobalt, Democratic Republic of Congo

(Received 16 February 2022; accepted 14 March 2022; Accepted Manuscript published online: 21 March 2022; Associate Editor: Anthony R Kampf)

Introduction

Cobalt is a relatively rare but important metal widely used in production of super alloys, special steel, carbides, diamond tools, magnets, rechargeable batteries and many others (USGS, 2022). It also plays a vital catalytic role in life evolution and biochemical synthesis (He *et al.*, 2021; Russell, 2022). In 2020, the worldwide mine production of cobalt amounted to 140,000 metric tons, with the biggest producer being the Democratic Republic of Congo (~95,000 tons), followed by Russia, Australia, Philippines, Cuba and Canada (Statista, 2021). In Nature, over 100 Co-bearing minerals have been identified, among which 66 mineral species have been approved by the Commission of New Minerals, Nomenclature and Classification of the International Mineralogical Association (IMA–CNMNC) (Hazen *et al.*, 2017). Natural cobalt oxide minerals are very rare (Hey, 1962). The spinel-structured Co^{2+}-oxide mineral cochromite, $(Co,Ni,Fe)(Cr,Al)_2O_4$, is one such, found in the Bon Accord nickel deposit, South Africa (De Waal, 1978). The Co^{3+} minerals such as linnaeite ($Co^{2+}Co_2^{3+}S_4$) and heterogenite ($Co^{3+}O(OH)$) also occur in some metal sulfide mines (Hey, 1962; Deliens and Goethals, 1973). Although synthetic Co_3O_4 has been studied widely (e.g. Natta and Schmidt, 1926; Hendriks and Albrecht, 1928; Osaki, 2018), and the existence of natural Co_3O_4 predicted by Hazen *et al.* (2017), its occurrence in Nature has not been reported until now.

During a mineralogical investigation on the cobalt ores from the Sicomines copper–cobalt mine, Democratic Republic of Congo, a mineral with the composition of Co_3O_4 was found, characterised, submitted to the Commission on New Minerals, Nomenclature and Classification of the International Mineralogical Association (IMA–CNMNC) and approved under IMA2017-080 (Lei *et al.*, 2017). The mineral name 'guite' (symbol Gui) is in honour of Prof. Xiangping Gu (1964–) of Central South University, Changsha, Hunan province, China. Prof. Gu obtained a BS degree in 1983 and a MS degree in 1986, both from the Central South University, and a DSc degree in 2003 from Hiroshima University in Japan. In the past 40 years he has made significant

*Author for correspondence: Jianxiong Wang, Email: wangerlang@163.com
Cite this article: Lei Z., Chen X., Wang J., Huang Y., Du F. and Yan Z. (2022) Guite, the spinel-structured $Co^{2+}Co_2^{3+}O_4$, a new mineral from the Sicomines copper–cobalt mine, Democratic Republic of Congo. *Mineralogical Magazine* **86**, 346–353. https://doi.org/10.1180/mgm.2022.27

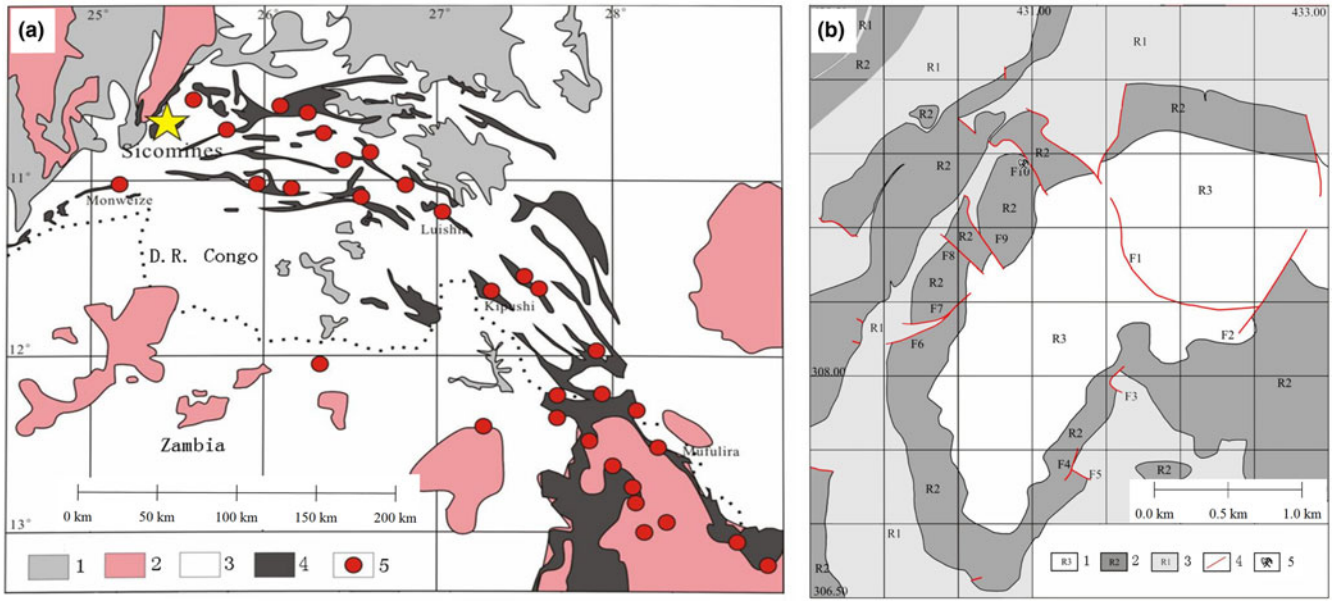

Fig. 1. (a) Simplified regional geological map of the Katanga Cu–Co belt and the location of the Sicomines mine (after Zhao, 2016). Legend: 1. Neozoic cover; 2. Basement strata; 3. Nguba and Kundelungu Formations; 4. Roan Formation; 5. Cu–Co deposits. (b) Plan geological map of the Sicomines Cu–Co deposit (after Chen *et al.*, 2012). Legend; 1: R3 Group of Roan Formation: dolomitic siltstone; 2: R2 Group of Roan Formation: talc-bearing argillaceous dolostone, silicified dolostone, dolomitic shale and siltstone; 3: R3 Group of Roan Formation: coarse-grained arkoses and conglomerate; 4: faults; 5: sampling locations.

contributions to mineralogical research and teaching in China; in particular to new mineral discoveries, and is the leading author of over 12, and the co-author of over 22 new minerals to date. The type material of guite is deposited in Geological Museum of China in Beijing with the catalogue number M13711 and a cotype sample is deposited at the RRUFF Project (deposition # R180022) (http://rruff.info).

Here, we present detailed descriptions of the morphology, composition, physical property, and crystallography of this mineral using optical microscopy, electron probe microanalysis (EPMA) and X-ray diffraction (XRD).

Occurrence and mineral association

Guite was found in the Sicomines copper-cobalt mine at 10°44'17.4"S, 25°22'50.4"E, ~11 km southwest of Kolwezi City, Democratic Republic of Congo. The Sicomines Cu–Co deposit is located at the northwest end of the world famous Katanga Cu–Co belt extending from Congo (Kinshasa) to Zambia (Fig. 1a). The Cu–Co ores are hosted in the Proterozoic Roan Formation, which is composed of red and grey–green sandstone and mudstone (R1 group), dolostone and dolomitic sandstone (R2 group) and dolomitic siltstone and mudstone (R3 group) (Fig. 1b). The Co-bearing dolomite in the R2 group is considered to be the source of cobalt (Chen *et al.*, 2012). The samples were taken from the drilling cores in the R2 group (Fig. 1b). Guite is supposed to be a supergene cobalt oxide formed from the precipitation of a cobalt-bearing solution at weakly alkaline and oxidising conditions:

$$3Co(HCO_3)_2 + \tfrac{1}{2}O_2 + 12OH^- \rightarrow Co_3O_4 + 6CO_3^{2-} + 9H_2O.$$

Appearance and physical properties

Guite occurs as granular aggregates up to 500 μm in size associated closely with heterogenite in quartz, in which anhedral to subhedral single crystals of guite are estimated to be several to tens of μm (Fig. 2). Guite has a dark grey colour with metallic opaque lustre and black streak. The Mohs hardness is estimated to be 6–6.5. The mineral is brittle with uneven fracture. The calculated density is of 6.003 g/cm^3 according to the empirical formula and unit cell volume from powder X-ray diffraction. Guite is non-magnetic as tested by a magnet needle.

In reflected light microscopy, guite has a white colour with no internal reflections. Zonar variation of reflectance and colour, from bright white (Fig. 2a,b) to brownish grey (Fig. 2c), is observed due to compositional zonation. The reflectance values (R, %) at different wavelength (λ, nm) measured using TIDAS MSP400 attached to LEICA DM2500p with SiC standard are shown in Table 1. The colour index is calculated relative to an equienergy lamp source. The data indicate that the reflectance of guite is ~25.4% for pure Co_3O_4 and apparently decreases to 22.9% when Cu, Mn and Si are incorporated (Table 1).

Chemical composition

The chemical composition of guite was determined on a Shimadzu EPMA-1720 microprobe by wavelength dispersive spectroscopy with operating conditions of accelerating voltage = 15 kV, beam current = 10 nA and beam size = 1 μm. Detectable elements include Co, Cu, Mn, Si and O; the contents of Fe, Mg, V and Ni are below the detection limits (~200 ppm) according to qualitative scans at specific wavelengths. Quantitative analysis was carried out using the following standards (and lines): pure Co (Co$K\alpha$); pure Cu (Cu$K\alpha$); pure Mn (Mn$K\alpha$); pure Si (Si$K\alpha$), and pure Fe_3O_4 (O$K\alpha$). The *ZAF4* correction program supplied with the instrument was used for the correction calculation. Compositional zoning is often observed (e.g. Fig 2c), mainly due to the variation of the contents of Cu (up to 2.50 wt.%) and Mn (up to 1.78 wt.%). The average of 20 electron-microprobe analyses is Co 71.53, Cu 0.58, Mn 0.67, Si 0.25, O 26.78, total 99.82 wt.%

https://doi.org/10.1180/mgm.2022.27 Published online by Cambridge University Press

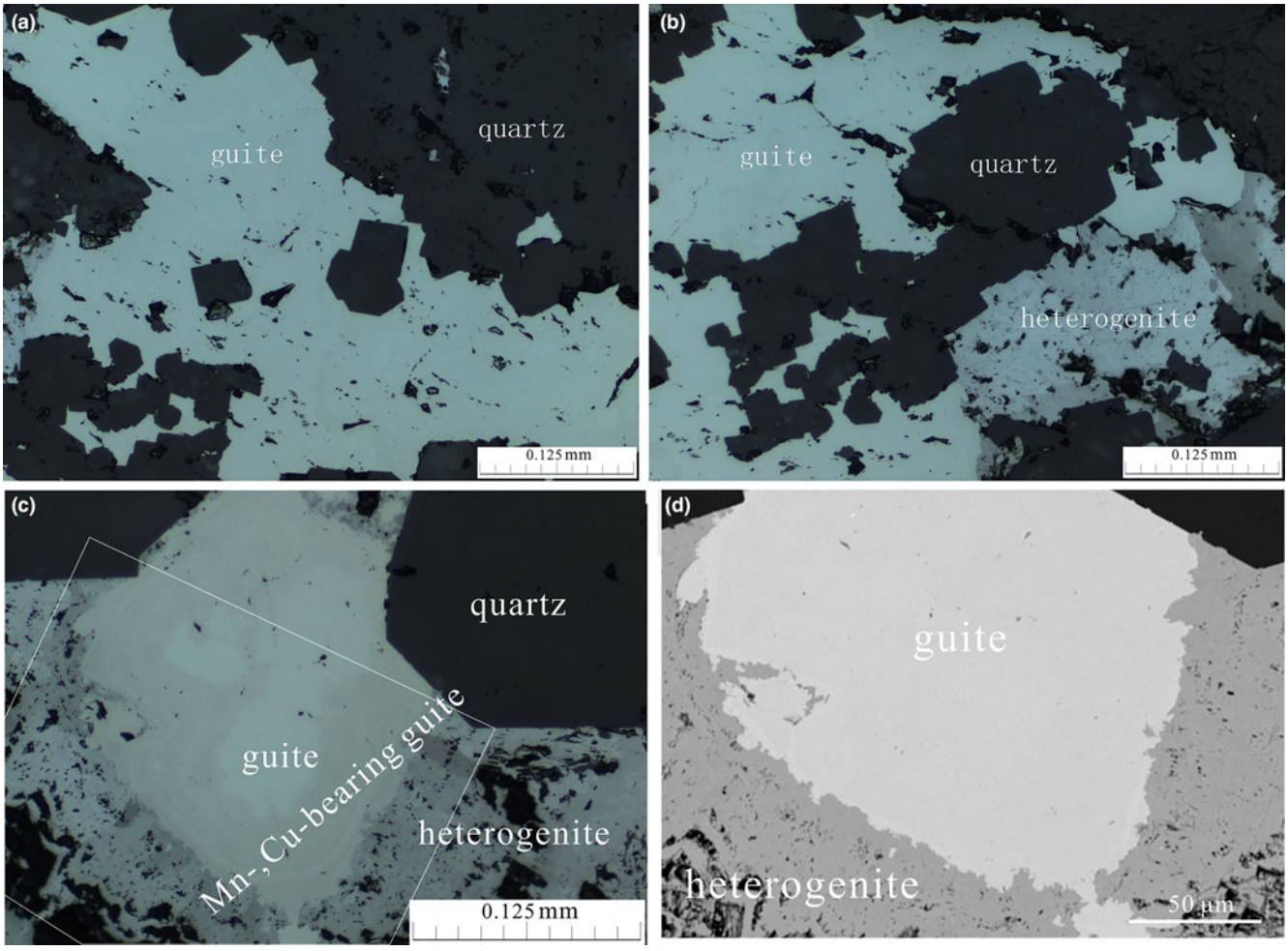

Fig. 2. Photomicrographs in reflected light (a–c) and back-scattered electron image (d) of guite. (a) Guite filling the interstitial space between quartz; (b) guite replaced by heterogenite in the interstitial space of quartz; (c) compositional zonation of guite – the core of almost pure Co_3O_4 surrounded by Mn-, Cu-bearing Co_3O_4, further replaced by heterogenite; and (d) back-scattered electron image of the area framed in (c).

Table 1. Reflectance data for guite.

$(Co_{0.98}Cu_{0.01}Si_{0.01})Co_2O_4$ [1]				$(Co_{0.72}Cu_{0.09}Mn_{0.08}Si_{0.03})Co_2O_4$ [2]			
λ (nm)	*R* (%)	λ (nm)	*R* (%)	λ (nm)	*R* (%)	λ (nm)	*R* (%)
400	25.6	560	25.5	400	22.6	560	22.9
420	25.8	580	25.3	420	22.8	580	22.8
440	25.9	**589**	**25.2**	440	23.0	**589**	**22.8**
460	25.9	600	25.1	460	23.1	600	22.7
470	**25.9**	620	24.8	**470**	**23.1**	620	22.6
480	25.9	640	24.5	480	23.1	640	22.5
500	25.8	**650**	**24.4**	500	23.1	**650**	**22.5**
520	25.8	660	24.2	520	23.1	660	22.5
540	25.6	680	23.9	540	23.0	680	22.4
546	**25.6**	700	23.6	**546**	**23.0**	700	22.4

Colour index:
[1] $x = 0.3298$, $y = 0.3325$, Y = 25.4, $\lambda_d = 480$ nm, Pe = 1.44%
[2] $x = 0.3320$, $y = 0.3335$, Y = 22.9, $\lambda_d = 481$ nm, Pe = 0.55%

(Table 2). The empirical formula calculated on the basis of 4 oxygen atoms per formula unit and with partitioning of Co^{2+} and Co^{3+} to achieve charge balance is: $(Co^{2+}_{0.92}Cu^{2+}_{0.02}Si^{4+}_{0.02})_{\Sigma 0.96}(Co^{3+}_{1.98}Mn^{3+}_{0.03})_{\Sigma 2.01}O_{4.00}$. The simplified formula is $(Co^{2+},Cu^{2+},Si^{4+})(Co^{3+},Mn^{3+})_2O_4$ and the ideal formula is $Co^{2+}Co^{3+}_2O_4$.

Table 2. Chemical data for guite (wt.%, *N* = 20).

Const.	Mean	Range	S.D.	Apfu	Probe standard
O	26.78	26.24–27.67	0.41	4.00	O*Kα* in pure Fe_3O_4
Co	71.53	71.53–73.47	1.40	2.90	Co*Kα* in pure Co
Si	0.25	0.05–0.57	0.13	0.02	Si*Kα* in pure Si
Mn	0.67	0.06–1.78	0.52	0.03	Mn*Kα* in pure Mn
Cu	0.58	0.16–2.50	0.54	0.02	Cu*Kα* in pure Cu
Total	99.82	98.60–101.37	0.74		

S.D. – standard deviation

Raman spectroscopy

Raman spectra of randomly oriented crystals of guite were measured at two laser wavelengths (532.1 and 632.8 nm) with a Horiba LabRam ARAMIS instrument (laser power = 5 mW, resolution = 2 cm^{-1} and scan time = 10 min). All the five theoretical Raman-active modes, calculated from the factor-group analysis on synthetic Co_3O_4 (Hadjiev *et al.*, 1988), are observed respectively at 197 (F_{2g}), 487 (E_g), 530 (F_{2g}), 625–630 (F_{2g}) and 693–697 (A_{1g}) cm^{-1} (Fig. 3). The Raman shifts may be attributed to the Co–O stretching vibration modes (500–700 cm^{-1}) and the O–Co–O bending vibration modes (100–500 cm^{-1}) in CoO_4

https://doi.org/10.1180/mgm.2022.27 Published online by Cambridge University Press

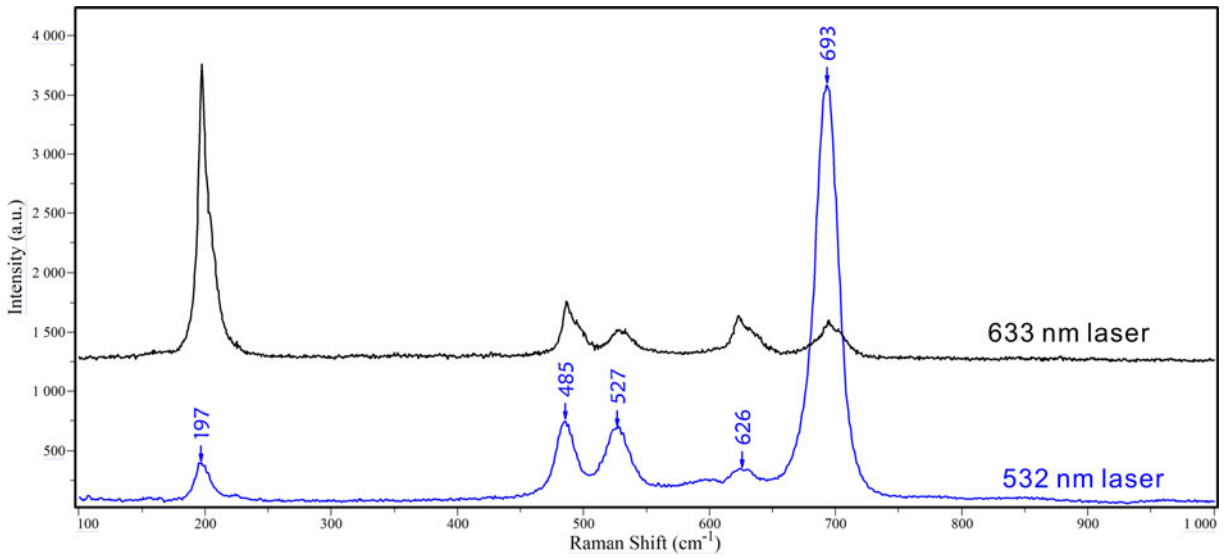

Fig. 3. Raman spectra of guite activated at two laser wavelengths.

Table 3. X-ray powder diffraction data (*I* in %, *d* in Å) for guite.*

$I_{cal.}$	$I_{obs.}$	$d_{cal.}$	$d_{obs.}$	*h k l*
15.7	**16.7**	**4.6677**	**4.6714**	**1 1 1**
29.3	**18.4**	**2.8584**	**2.8620**	**2 2 0**
100	**100.0**	**2.4376**	**2.4399**	**3 1 1**
11.1	**10.4**	**2.3339**	**2.3348**	**2 2 2**
20.3	**24.8**	**2.0212**	**2.0230**	**4 0 0**
8.9	7.5	1.6503	1.6517	4 2 2
30.5	**26.3**	**1.5559**	**1.5556**	**5 1 1, 3 3 3**
40.9	**37.7**	**1.4292**	**1.4296**	**4 4 0**
1.8	2.4	1.3666	1.3669	5 3 1
3	3.5	1.2783	1.2782	6 2 0
9.3	6.8	1.2329	1.2328	5 3 3
5.7	4.0	1.2188	1.2189	6 2 2
2.7	2.5	1.1669	1.1663	4 4 4
1.1	1.3	1.1321	1.1319	7 1 1, 1 5 5
4.4	3.5	1.0804	1.0802	6 4 2
8.1	**10.1**	**1.0525**	**1.0524**	**7 3 1, 3 5 5**
5.7	4.6	1.0106	1.0103	8 0 0
1.5	2.6	0.9528	0.9521	8 2 2, 0 6 6
8.8	5.9	0.9335	0.9335	7 5 1, 5 5 5
3.5	2.9	0.9274	0.9281	6 6 2
4.2	3.0	0.9039	0.9039	8 4 0

*The strongest lines are given in bold.

tetrahedra and CoO_6 octahedra. The relative intensities of peaks vary for different laser wavelengths. The spectrum of 532.1 nm has the strongest peak at 693–697 (A_{1g}) cm^{-1} and the spectrum of 632.8 nm has the strongest peak at 197 (F_{2g}) cm^{-1}.

Crystallography and crystal structure

Powder X-Kray diffraction data were obtained respectively using a Rigaku D/Max Rapid IIR diffractometer (Cu*K*α; 40 kV; 250 mA; 0.1 mm beam diameter; and exposure time of 1 hour) and a Rigaku Synergy single-crystal diffractometer in Gandolfi powder mode (Mo*K*α; 50 kV; 1 mA; 0.2 mm beam diameter; and exposure time of 20 min). The reflection data are given in Table 3. The eight strongest lines [*d* in Å (I/I_0) (*hkl*)] are: 4.6714 (16.7) (111), 2.8620 (18.4) (220), 2.4399 (100) (311), 2.3348 (10.4) (222), 2.0230 (24.8) (400), 1.5556 (26.3) (511, 333), 1.4296 (37.7) (440) and 1.0524 (10.1) (731, 553). The unit cell parameters refined from the powder X-ray diffraction data are: a =8.0848 (1) Å, V = 528.45(2) Å^3 and Z = 8. The calculated density of guite is 6.003 g/cm^3 according to the empirical formula.

Table 4. Information on crystal and structural refinement for guite.

Crystal data	
Empirical formula	$Co_{2.90}Mn_{0.03}Cu_{0.02}Si_{0.02}O_{4.00}$
Formula weight	238.38
Crystal size (mm)	0.01 × 0.008 × 0.006
Crystal system	isometric
Space group	$Fd\bar{3}m$ (#227)
Unit cell dimensions (Å)	a = 8.0898(1)
Volume (Å^3)	529.44(2)
Z	8
Calculated density (g/cm^3)	5.981
Data collection	
Instrument	Rigaku Synergy
Temperature (K)	293(2)
Radiation, wavelength (Å)	Mo*K*α, 0.71073
2θ range (°)	8.728 to 66.308
μ (mm^{-1})	18.071
F(000)	895.0
Total reflections	3748
Unique reflections (all)	69
Unique reflections [$I > 4\sigma(I)$]	66
R_{int}	0.0262
R_σ	0.0055
Range of *h*, *k*, *l*	$-12 \le h \le 12$; $-12 \le k \le 12$; $-11 \le l \le 11$
Refinement	
R_1, wR_2 [$I > 4\sigma(I)$]	R_1 = 0.0124, wR_2 = 0.0349
R_1, wR_2 [all data]	R_1 = 0.0132, wR_2 = 0.0352
Goodness-of-fit	1.258
No. of parameters, restraints	7, 0
Largest diff. peak/hole (e^-Å^{-3})	0.49/–0.41

The single-crystal X-ray diffraction data for a guite crystal, ~10 μm in size, were collected on Rigaku XtaLAB Synergy-DS diffractometer with microfocus sealed Mo anode tube at 50 kV, 1 mA and 25 s of frame exposure time. The diffraction data were processed with the Rigaku program *CrysAlisPro*. The crystal structure was determined and refined using *SHELX* (Sheldrick, 2015a,b) included in the software *Olex2* (Dolomanov *et al.*, 2009). The crystallographic data and refinement statistics are given in

https://doi.org/10.1180/mgm.2022.27 Published online by Cambridge University Press

Table 5. Atomic coordinates and displacement parameters (in Å^2) for guite.*

Site	Atom	Wyckoff	*x*	*y*	*z*	U_{eq}	U^{11}	U^{22}	U^{33}	U^{23}	U^{13}	U^{12}
Co1	Co^{2+}	8*a*	⅜	⅜	⅞	0.0046(2)	0.0046(2)	U^{11}	U^{11}	0	U^{23}	U^{23}
Co2	Co^{3+}	16*d*	½	½	½	0.0036(2)	0.0036(2)	U^{11}	U^{11}	−0.00012(9)	U^{23}	U^{23}
O1	O^{2-}	32*e*	0.51356(16)	0.51356(16)	0.73644(16)	0.0053(4)	0.0053(4)	U^{11}	U^{11}	0.0001(4)	U^{23}	U^{23}

*Occupancies: Co1: $Co_{0.92}Si_{0.02}Cu_{0.02}Mn_{0.01}$; Co2 $Co_{0.99}Mn_{0.01}$; O1: $O_{1.00}$

Table 6. Selected bond distances and angles for guite.

Co-O4 tetrahedra	*d* (Å)	Co-O6 triprism	*d* (Å)
Co1–O1 ×4	1.942(2)	Co2–O1 ×6	1.919(1)
O1–O1	3.170(3) ×6	O1–O1	2.550(3) ×6, 2.869(3) ×6
Co1–Co1	3.50299(5)	Co2–Co2	2.86018(4)
Co1–Co2	3.35385(5)		
Bond	**Angle (°)**	**Bond**	**Angle (°)**
O1–Co1–O1	109.47(4)	O1–Co2–O1	83.27(8), 96.73(6)
		Co2–O1–Co2	96.35(6)

Table 7. Calculated bond-valence sums (in valence units) for atoms in guite.*

	Co1	Co2	Sum	Ideal
O1	$0.505^{\times 4\downarrow \times 1\rightarrow}$	$0.509^{\times 6\downarrow \times 3\rightarrow}$	2.032	2
Sum	2.021	3.053		
Ideal	2	3		

*Bond-valence parameters were taken from Brese and O'Keeffe (1991)

Table 4. The structure was solved in space group $Fd\bar{3}m$ and refined with anisotropic displacement for all sites. The occupancies of Co, Cu, Mn and Si at the Co1 and Co2 sites were fixed manually according to empirical formula from the chemical compositions. The final anisotropic full-matrix least-squares refinement on F^2 for 7 parameters was completed with $R_1 = 1.32\%$ and $wR_2 = 3.52\%$ for all 2007 (69 unique) reflections. The atomic coordinates and displacement parameters are listed in Table 5, and selected bond lengths and angles in Table 6. The bond-valence sums of atoms, calculated according to the actual composition using the parameters given by Brese and O'Keeffe (1991), are presented in Table 7. The structure is illustrated in Fig. 4. The crystallographic information files have been deposited with the Principal Editor of *Mineralogical Magazine* and are available as Supplementary material (see below).

Guite has the spinel-type structure in which the Co1 site is in tetrahedral coordination and occupied by Co^{2+} with a Co–O distance of 1.942 Å, and the Co2 site is in octahedral coordination and occupied by Co^{3+} with a Co–O distance of 1.919 Å (Table 6). In compliance with the site symmetry $\bar{3}m$, the six faces of Co^{3+}–O_6 octahedra are composed of two equilateral

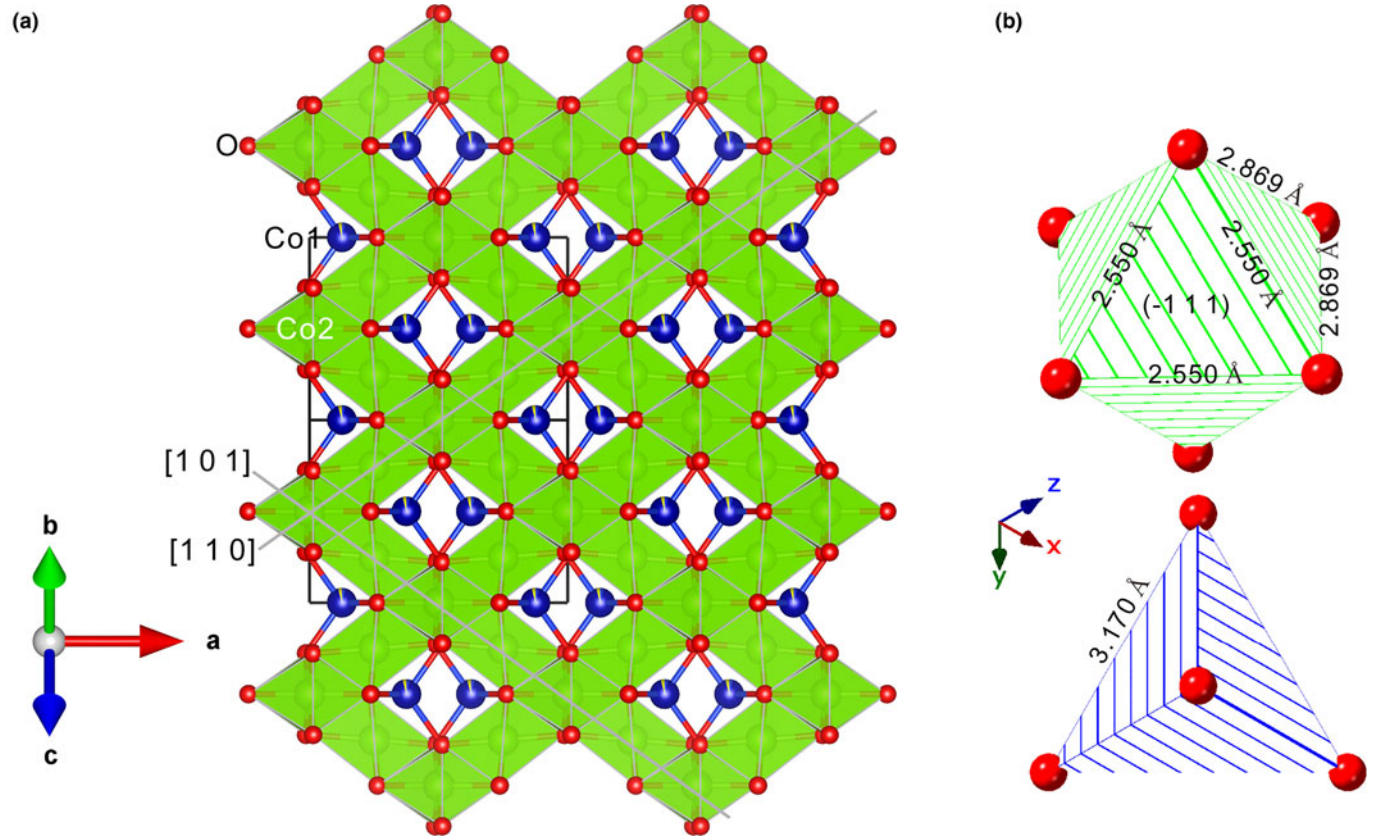

Fig. 4. (a) Crystal structure of guite viewed in [0 1 1], showing the chains of CoO_6 octahedra (green) along the directions [0 1 1], [1 0 1] and [1 1 0] with isolated CoO_4 tetrahedra (blue) occupying the interstitial space of the chains. (b) The shape and edge lengths of CoO_6 octahedra (twisted triprism) and CoO_4 tetrahedra.

https://doi.org/10.1180/mgm.2022.27 Published online by Cambridge University Press

Table 8. Unit cell data, calculated density, bonding lengths in tetrahedra and octahedra, and reflectance of the minerals and high pressure phases in the oxyspinel group.

Mineral	Formula	Space group	Unit cell, *a* (Å)	Density (g/cm^3)	M_{tet}–O (Å)	M_{oct}–O (Å)	R_{rgb} (%)	Ref.
Guite	$Co^{2+}Co_2^{3+}O_4$	Fd$\bar{3}$m	8.085	6.00	1.942	1.919	25.5	1
Synthetic guite	$CoCo_2O_4$	Fd$\bar{3}$m	8.084	6.06	1.942	1.917		2
Spinel	$MgAl_2O_4$	*Fd$\bar{3}$m*	8.085	3.58	1.919	1.929		3
Dellagiustaite	$V^{2+}Al_2O_4$	*Fd$\bar{3}$m*	8.195	4.60	1.782	2.045		4
Galaxite	$MnAl_2O_4$	Fd$\bar{3}$m	8.210	4.15	2.004	1.931		5
Hercynite	$Fe^{2+}Al_2O4$	Fd$\bar{3}$m	8.156	4.26	1.953	1.937		6
Thermaerogenite	$CuAl_2O_4$	*Fd$\bar{3}$m*	8.078	4.57	1.903	1.935		7
Gahnite	$ZnAl_2O_4$	*Fd$\bar{3}$m*	8.083	4.61	1.956	1.909		8
Chukochenite	$LiAl_5O_8$	Imma	*a*=5.657, *b*=16.892, *c*=7.992	3.74	1.811/ 1.929	1.904/ 1.922/ 2.008		9
Magnesiocoulsonite	$MgV_2^{3+}O_4$	*Fd$\bar{3}$m*	8.385	4.29	1.961	2.016		10
Vuorelainenite	$Mn^{2+}V_2^{3+}O_4$	*Fd$\bar{3}$m*	8.520	4.74	2.041	2.023		11
Coulsonite	$FeV_2^{3+}O_4$	*Fd$\bar{3}$m*	8.543	4.72	2.012	2.046		12
Magnesiochromite	$MgCr_2O_4$	Fd$\bar{3}$m	8.334	4.41	1.970	1.992		13
Manganochromite	$Mn^{2+}Cr_2O_4$	Fd$\bar{3}$m	8.437	4.93	2.034	1.997		14
Chromite	$Fe^{2+}Cr_2O_4$	*Fd$\bar{3}$m*	8.383	5.05	1.995	1.997	12.1	15
			a=9.715, *b*=2.870, *c*=9.490	5.27				16
Chenmingite*	$Fe^{2+}Cr_2O_4$	Pnma						
Xieite*	$Fe^{2+}Cr_2O_4$	Bbmm	*a*=9.462, *b*=9.562, *c*=2.916	5.34		1.997/ 2.205	15.3	17
Cochromite	$Co^{2+}Cr_2O_4$	*Fd$\bar{3}$m*	8.333	5.21	1.986	1.984	14.0	18
Nichromite	$NiCr_2O_4$	*Fd$\bar{3}$m*	8.309	5.25	1.964	1.987		19
Zincochromite	$ZnCr_2O_4$	*Fd$\bar{3}$m*	8.327	5.37	1.971	1.989	11.9	20
Magnesioferrite	$MgFe_2^{3+}O4$	*Fd$\bar{3}$m*	8.393	4.49	1.904	2.049	18.7	21
Maohokite*	$MgFe_2^{3+}O_4$	Pnma	*a*=8.907, *b*=9.937, *c*=2.981	5.33				22
Jacobsite	$Mn^{2+}Fe_2^{3+}O_4$	*Fd$\bar{3}$m*	8.356	5.25	1.976	1.998	17.5	23
Magnetite	$Fe^{2+}Fe_2^{3+}O_4$	*Fd$\bar{3}$m*	8.400	5.06	1.887	2.061	20.7	24
Trevorite	$NiFe_2^{3+}O_4$	Fd$\bar{3}$m	8.334	5.34	1.846	2.060		25
Cuprospinel	$CuFe_2^{3+}O_4$	*Fd$\bar{3}$m*	8.404	5.35	1.921	2.044	21.4	26
Franklinite	$ZnFe_2^{3+}O_4$	Fd$\bar{3}$m	8.443	5.32	1.979	2.028	17.9	27
Ahrensite*	$SiMg_2O_4$	*Fd$\bar{3}$m*	8.065	3.56	1.654	2.071		28
Ringwoodite*	$SiFe_2^{2+}O_4$	Fd$\bar{3}$m	8.234	4.85	1.652	2.137		29
Ulvöspinel	$Fe^{2+}(TiFe^{2+})O_4$	*Fd$\bar{3}$m*	8.521	4.80	2.007	2.041	18.1	30
Brunogeierite	$Ge^{4+}Fe_2^{2+}O_4$	*Fd$\bar{3}$m*	8.409	5.51	1.813	2.107	13.3	31
Filipstadite	$(Fe_{0.5}^{3+}Sb_{0.5}^{5+})Mn_2O_4$	Fd$\bar{3}$m	25.930	4.90	1.990	2.061	11.8	32
Qandilite	$(Ti,Fe^{3+})(Mg,Fe^{3+})_2O_4$	Fd$\bar{3}$m	8.495	4.03	1.990	2.034	13.3	33
Maghemite	$(Fe_{0.67}^{3+}\square_{0.33})Fe_2^{3+}O_4$	*P*4$_3$32	8.336	4.86	1.886	2.032	24.8	34
Titanomaghemite	$(Ti_{0.5}^{4+}\square_{0.5})Fe_2^{3+}O_4$	*P*4$_3$32	8.341	4.70	1.879	2.020		35
Hausmannite	$Mn^{2+}Mn_2^{3+}O_4$	I4$_1$/amd	*a*=5.765, *c*=9.442	4.84	2.040	2.047	16.0/ 20.1	36
Hetaerolite	$ZnMn_2^{3+}O_4$	I4$_1$/amd	*a*=5.72, *c*=9.24	5.26	1.985	2.037	14.5/ 18.5	37

*high-pressure phase. 1. This work; 2. Knop *et al.* (1968); 3. Fregola *et al.* (2012); 4. Cámara *et al.* (2019); 5. Nair *et al.* (2014); 6. Palache *et al.* (1944), Hill (1984); 7. Cooley and Reed (1972); 8. Verger *et al.* (2016); 9. Rao (pers. Comm.); 10. Reznitskii *et al.* (1995); 11. Plumier (1962); 12. Reuter *et al.* (1969); 13. O'Neill *et al.* (1994); 14. Hastings and Corliss (1962); 15. Palache *et al.* (1944), Kyono *et al.* (2012); 16. Ma *et al.* (2019); 17. Ishii *et al.* (2014); Chen *et al.* (2008); 18. De Waal (1978), Hirota *et al.* (1990); 19. Ueno *et al.* (1999); 20. Nesterov and Rumyantseva (1987), Bosi *et al.* (2011); 21. Palache *et al.* (1944), Gaudon *et al.* (2009); 22. Chen *et al.* (2018); 23. Rashmi *et al.* (2017); 24. Palache *et al.* (1944); 25. Kiselev *et al.* (2007); 26. Ahmed *et al.* (2012); 27. Waerenborgh *et al.* (1994); 28. Sasaki *et al.* (1982); 29. Yagi *et al.* (1974); 30. Forster and Hall (1965); 31. Ottemann and Nuber (1972), Welch *et al.* (2001); 32. Bonazzi *et al.* (2013), Dunn *et al.* (1988); 33. Bosi *et al.* (2014); 34. Solano *et al.* (2014); Bozi *et al.* (2019); 35. Collyer *et al.* (1988); Bozi *et al.* (2019); 36. Jarosch (1987); and 37. Yamamoto *et al.* (1983).

triangles with the O–O distance of 2.550 Å and four isosceles triangles comprising two O–O of 2.689 Å and one O–O of 2.550 Å, which may be described more precisely by a twisted triprism (Fig. 4b). The Co^{3+}–O_6 octahedra share the edges at 2.550 Å to form a framework of chains of octahedra in three directions of [0 1 1], [1 1 0] and [1 0 1] with Co^{2+} occupying the interstitial spaces in tetrahedral coordination among the chains (Fig. 4a). The valence states of Co^{2+} at the Co1 site and Co^{3+} at the Co2 site are confirmed by the bond valence sums of the two sites (Table 7), and the different Co–O bonding lengths of the two sites (1.942 *vs.* 1.919 Å) suggest a high spin electronic structure for Co^{2+} and a low spin electronic structure for Co^{3+} according to the ionic radii of Shannon (1976).

Discussions and implications

In literature, numerous structural and physico-chemical data of synthetic Co_3O_4 have been reported (e.g. Natta and Schmidt, 1926; Hendriks and Albrecht, 1928; Liu and Prewitt, 1990; Douin *et al.*, 2009; Osaki, 2018). All of them have the spinel structure with highly ordered occupation of Co^{2+} in the tetrahedral site and Co^{3+} in the octahedral site at room temperature and ambient atmosphere, with the unit cell *a* ranging from 8.065 Å to 8.086 Å, the Co–O_{tet} bonding lengths in CoO_4 tetrahedra from 1.908 Å to 1.988 Å and the Co–O_{oct} bonding lengths in CoO_6 octahedra from 1.893 Å to 1.933 Å. A linear regression between Co–O_{tet} and Co–O_{oct} yields:

$$\text{Co–O}_{oct} = -0.4774 \times \text{Co–O}_{tet} + 2.8431 \ (R^2 = 0.9667, N = 9).$$

The negative correlation between Co–O_{tet} and Co–O_{oct} seems to indicate a variation of Co^{2+}–Co^{3+} distribution between the tetrahedral site and the octahedral site. On the other hand, the high-temperature structural determinations of synthetic Co_3O_4 indicated a tendency of disorder of Co^{2+}–Co^{3+} distribution between the tetrahedral site and the octahedral site at high temperatures (e.g. Liu and Prewitt, 1990; Hazen and Yang, 1999; Douin *et al.*, 2009).

https://doi.org/10.1180/mgm.2022.27 Published online by Cambridge University Press

Guite is a member of the oxyspinel group in the spinel supergroup (Bosi *et al.*, 2019), which may be classified into Al-, V-, Cr-, Fe-, Co-subgroups according to the elements in the octahedral site, with various end-members of Mg, Si, V, Mn, Fe, Co, Cu, Zn, Ge and Sb occupying the tetrahedral site. The spinel structure is of special significance for probing the material states in the deep mantle (e.g. Hazen and Yang, 1999). As summarised and compared in Table 8, guite is outstanding in the group as it has the smallest unit cell, the biggest density and the highest reflectance. The presence of Si (up to 0.02 apfu), Mn (up to 0.08 apfu) and Cu (up to 0.09 apfu) in guite may predict the natural existence of end members $SiCo_2^{2+}O_4$, $Mn^{2+}Co_2^{3+}O_4$ and $CuCo_2^{3+}O_4$, which have been synthesised in the laboratory (e.g. Morimoto *et al.*, 1974; Gautier *et al.*, 1982; Petrov *et al.*, 1989). It is interesting to note that hausmannite ($Mn^{2+}Mn_2^{3+}O_4$) and hetaerolite ($ZnMn_2^{3+}O_4$) adopt a tetragonal structure, topologically similar to the spinel-type structure (Yamamoto *et al.*, 1983; Jarosch, 1987). The high-pressure transformation of guite, such as that of chromite to xieite and chenmingite (Chen *et al.*, 2008; Ma *et al.*, 2019) and magnesioferrite to maohokite (Chen *et al.*, 2018), is still unknown though it has been shown to be stable up to 1201 K and 8.7 GPa (e.g. Liu and Prewitt, 1990; Golosova *et al.*, 2020).

In the Li-ion batteries industry, synthetic Co_3O_4 has attracted wide attention as an anode material for its low cost and high theoretical capacity (890 mA h/g) (e.g. Zhang *et al.*, 2017; Xiao *et al.*, 2018). In the Sicomines mine, guite is an important economic mineral and accounts for about one-fifth of the cobalt resource; this discovery of guite originated from the work to increase the recovery rate of cobalt from the ores.

Acknowledgements. The authors thank Prof. Xiande Xie of Guangzhou Institute of Geochemistry, Chinese Academy of Science, for his help in preparing the manuscript, and Prof. Xiangping Gu of Central South University for his assistance in microprobe analyses and structural determination. The manuscript was improved from the comments of Prof. Peter Leverett, Dr. Fernando Camara and an anonymous reviewer.

Supplementary material. To view supplementary material for this article, please visit https://doi.org/10.1180/mgm.2022.27

References

Ahmed M.A., Afify H.H., El Zawawia I.K. and Azab A.A. (2012) Novel structural and magnetic properties of Mg doped copper nanoferrites prepared by conventional and wet methods. *Journal of Magnetism and Magnetic Materials*, **324**, 2199–2204.

Bonazzi P., Chelazzi L. and Bindi L. (2013) Superstructure, crystal chemistry, and cation distribution in filipstadite, a Sb^{5+}-bearing, spinel-related mineral. *American Mineralogist*, **98**, 361–366.

Bosi, F. Andreozzi, G.B. Halenius, U. and Skogby, H. (2011) Zn-O tetrahedral bond length variations in normal spinel oxides. *American Mineralogist*, **96**, 594–598.

Bosi F., Hålenius U. and Skogby H. (2014) Crystal chemistry of the ulvöspinel-qandilite series. *American Mineralogist*, **99**, 847–851.

Bosi F., Biagioni C. and Pasero M. (2019) Nomenclature and classification of the spinel supergroup. *European Journal of Mineralogy*, **31**, 183–192.

Brese N.E. and O'Keeffe M. (1991) Bond-valence parameters for solids. *Acta Crystallographica*, **B47**, 192–197.

Cámara F., Bindi L., Pagano A., Pagano R., Gain S.E.M. and Griffin W.L. (2019) Dellagiustaite: a novel natural spinel containing V^{2+}. *Minerals*, **9**, 1–16.

Chen M., Shu J. and Mao H. (2008) Xieite, a new mineral of high pressure $FeCr_2O_4$ polymorph. *Chinese Science Bulletin*, **53**, 3341–3345.

Chen X.H., Liu Y.J., Yang Y., Wang J.K., He Y. and Li T.Q. (2012) Geological characteristics and genesis of Sicomines copper-cobalt deposit in D.R. Congo. *Nonferrous Metals* (*Ser. Mines*), **64**, 31–37 [in Chinese with English abstract]

Chen M., Shu J., Xie X. and Tan D. (2018) Maohokite, a post-spinel polymorph of $MgFe_2O_4$ in shocked gneiss from the Xiuyan crater in China. *Meteoritics & Planetary Science*, **54**, 1–8.

Collyer S., Grimes N.W., Vaughan D.J. and Longworth G. (1988) Studies of the crystal structure and crystal chemistry of titanomaghemite. *American Mineralogist*, **73**, 153–160.

Cooley R.F. and Reed J.S. (1972) Equilibrium cation distribution in $NiAl_2O_4$, $CuAl_2O_4$, and $ZnAl_2O_4$ spinels. *Journal of the American Ceramic Society*, **55**, 395–398.

De Waal S.A. (1978) Nickel minerals from Barberton, South Africa: VIII. The spinels cochromite and nichromite, and their significance to the origin of the Bon Accord nickel deposit. *Bulletin BRGM, Géologie des Gîtes Minéraux*, **3**, 225–230.

Deliens M. and Goethals H. (1973) Polytypism of heterogenite. *Mineralogical Magazine*, **39**, 152–157.

Dolomanov O.V., Bourhis L.J., Gildea R.J., Howard, J.A.K. and Puschmann, H. (2009) A complete structure solution, refinement and analysis program. *Journal of Applied Crystallography*, **42**, 339–341.

Douin M., Guerlou Demourgues L., Menetrier M., Bekaert E., Goubault L., Bernard P. and Delmas C. (2009) Improvement by heating of the electronic conductivity of cobalt spinel phases, electrochemically synthesized in various electrolytes. *Journal of Solid State Chemistry*, **182**, 1273–1280.

Dunn P.J., Peacor D.R., Criddle A.J. and Stanley C.J. (1988) Filipstadite, a new Mn-Fe^{3+}-Sb derivative of spinel from Lanban, Sweden. *American Mineralogist*, **73**, 413–419.

Forster R.H. and Hall E.O. (1965) A neutron and X-ray diffraction study of ulvöspinel, Fe_2TiO_4. *Acta Crystallographica*, **18**, 859–862.

Fregola R.A., Bosi F., Skogby H. and Halenius U. (2012) Cation ordering over short-range and long-range scales in the $MgAl_2O_4$–$CuAl_2O_4$ series. *American Mineralogist*, **97**, 1821–1827.

Gaudon M., Pailhe N., Wattiaux A. and Demourgues A. (2009) Structural defects in AFe_2O_4 (A = Zn, Mg) spinels. *Materials Research Bulletin*, **44**, 479–484.

Gautier J.L., Barbato S., Brenet J. (1982) Ionic repartition in the manganese cobaltite. *Comptes Rendus des Seances de l'Academie des Sciences, Serie C: Sciences Chimiques*, **294**, 427–430.

Golosova N.O., Kozlenko D.P., Nicheva D. and Savenko B.N. (2020) High pressure effects on the crystal and magnetic structures of Co_3O_4. *Journal of Magnetism and Magnetic Materials*, **508**, 166874.

Hadjiev V.G., Ilievl M. N. and Vergilov I.V. (1988) The Raman spectra of Co_3O_4. *Journal of Physics C*, **21**, l99–201.

Hastings J.M. and Corliss L.M. (1962) Magnetic structure of manganese chromite. *Physical Review*, **126**, 556–565.

Hazen R.M. and Yang H.X. (1999) Effects of cation substitution and order-disorder on P-V-T equations of state of cubic spinels. *American Mineralogist*, **84**, 1956–1960.

Hazen R.T., Hystad G.J., Golden J., Hummer D.R., Liu C.R., Downs T., Morrison S.M., Ralph J. and Grew E.S. (2017) Cobalt mineral ecology. *American Mineralogist*, **102**, 108–116.

He D.P., Wang X.G., Yang Y., He R.T., Zhong H., Wang Y., Han B.X. and Jin F.M. (2021) Hydrothermal synthesis of long-chain hydrocarbons up to C_{24} with $NaHCO_3$-assisted stabilizing cobalt. *PNAS*, **118**, e2115059118.

Hendriks S.B. and Albrecht W.H. (1928) Roentgenographische und chemische Untersuchungen an einigen Oxyden des Eisens und Kobalts. *Berichte der deutschen Chemischen Gesellschaft*, **61**, 2153–2161.

Hey M. (1962) Cobaltic hydroxide in nature. *Mineralogical Magazine*, **33**, 253–259.

Hill R.J. (1984) X-ray powder diffraction profile refinement of synthetic hercynite. *American Mineralogist*, **69**, 937–942.

Hirota K., Inoue T., Mochida N. and Ohtsuka A. (1990) Study of germanium spinels (Part 3). *Nippon Seramikkusu Kyokai Gakujutsu Ronbunshi*, **98**, 976–986.

Ishii T., Kojitani H., Tsukamoto S., Fujino K., Mori D., Inaguma Y., Tsujino N., Yoshino T., Yamazaki D., Higo Y., Funakoshi K. and Akaogi M. (2014) High-pressure phase transitions in $FeCr_2O_4$ and structure analysis of new post-spinel $FeCr_2O_4$ and $Fe_2Cr_2O_5$ phases with meteoritical and petrological implications. *American Mineralogist*, **99**, 1788–1797.

Jarosch D. (1987) Crystal structure refinement and reflectance measurements of hausmannite, Mn_3O_4. *Mineralogy and Petrology*, **37**, 15–23.

Kiselev E.A., Proskurnina N.V., Voronin V.I. and Cherepanov V.A. (2007) Phase equilibria and crystal structures of phases in the La–Fe–Ni–O system at 1370 K in air. *Neorganicheskie Materialy*, **43**, 209–217.

Knop O., Reid K.I.G., Sutarno R. and Nakagawa Y. (1968) Chalkogenides of the transition elements. VI. X-Ray, neutron, and magnetic investigation of the spinels Co_3O_4, $NiCo_2O_4$, Co_3S_4, and $NiCo_2S_4$. *Canadian Journal of Chemistry*, **46**, 3463–3476.

Kyono A., Gramsch S.A., Yamanaka T., Ikuta D., Ahart M., Mysen B.O., Mao H.K. and Hemley R.J. (2012) The influence of the Jahn-Teller effect at $Fe^{(2+)}$ on the structure of chromite at high pressure. *Physics and Chemistry of Minerals*, **39**, 131–141.

Lei Z., Chen X., Wang J., Zhang J., Huang Y., Lu Z. and Du F. (2017) Guite, IMA 2017-080. CNMNC Newsletter No. 40, December 2017, page 1581. *Mineralogical Magazine*, **81**, 1577–1581.

Liu X. and Prewitt C.T. (1990) High-temperature X-ray diffraction study of Co_3O_4: transition from normal to disordered spinel. *Physics and Chemistry of Minerals*, **17**, 168–172.

Ma C., Tschauner O., Beckett J.R., Liu Y., Greenberg E. and Prakapenka V.B. (2019) Chenmingite, $FeCr_2O_4$ in the $CaFe_2O_4$-type structure, a shock-induced, high-pressure mineral in the Tissint martian meteorite. *American Mineralogist*, **104**, 1521–1529.

Morimoto N., Tokonami M., Watanabe M. and Koto K. (1974) Crystal structures of three polymorphs of Co_2SiO_4. *American Mineralogist*, **59**, 475–485.

Nair H.S., Fu Z.D., Voigt J., Su Y.X. and Brueckel Th. (2014) Approaching the true ground state of frustrated A-site spinels: a combined magnetization and polarized neutron scattering study. *Physical Review B*, **89**, 1–9.

Natta G. and Schmidt F. (1926) Oxides and hydrates of cobalt. *Atti della Accademia Nazionale dei Lincei, Classe di Scienze Fisiche, Matematiche e Naturali, Rendiconti, Serie 7*, **4**, 145–149.

Nesterov A.R. and Rumyantseva Y.V. (1987) Zincochromite $ZnCr_2O_4$ – a new mineral from Karelia. *Zapiski Vsesoyuznogo Mineralogicheskogo Obshchestva*, **116**, 367–371 [in Russian with English abstract].

O'Neill H.St.C. and Dollase W.A. (1994) Crystal structures and cation distributions in simple spinels from powder XRD structural refinements: $MgCr_2O_4$, $ZnCr_2O_4$, Fe_3O_4 and the temperature dependence of the cation distributionin $ZnAl_2O_4$. *Physics and Chemistry of Minerals*, **20**, 541–555.

Osaki T. (2018) Synthesis of $Zn_xCo_{3-x}O_4$ spinels at low temperature and atmospheric pressure. *Journal of Materials Science*, **53**, 3250–3266.

Ottemann J. and Nuber B. (1972) Brunogeierite, ein Germanium-Ferritspinell von Tsumeb. *Neues Jahrbuch fuer Mineralogie, Monatshefte*, **2**, 263–267.

Palache C., Berman H. and Frondel C. (1944) *Dana's System of Mineralogy, 7th edition, vol. I*. John Wiley and Sons, Inc., New York [pp 689–697].

Petrov K., Krezhov K. and Konstantinov P. (1989) Neutron diffraction study of the cationic distribution In $Cu_xCo_{3-x}O_4$ ($0<x<=1.0$) spinels prepared by thermal decomposition of layered hydroxide nitrate precursors. *Journal of Physics and Chemistry of Solids*, **50**, 577–581.

Plumier R. (1962) Etude par diffraction des neutrons du compose spinelle MnV_2O_4. *Comptes Rendus Hebdomadaires des Seances de l'Academie des Sciences*, **255**, 2244–2246.

Rashmi S.K., Naik H.S.B., Jayadevappa H., Sudhamani C.N., Patil S.B. and Naik M.M. (2017) Influence of Sm^{3+} ions on structural, optical and solar light driven photocatalytic activity of spinel $MnFe_2O_4$ nanoparticles. *Journal of Solid State Chemistry*, **255**, 178–192.

Reuter B., Riedel E., Hug P., Arndt D., Geisler U. and Behnke J. (1969) Zur Kristallchemie der Vanadin(III)-Spinelle. *Zeitschrift fur Anorganische und Allgemeine Chemie*, **369**, 306–312.

Reznitskii L.Z., Sklyaov E.V. and Ushchapovskaya Z.F. (1995) Magnesiocoulsonite – a new meneral species in the spinel group. *Zapiski Vserossiiskogo Mineralogicheskogo Obshchestva*, **124**, 91–97.

Russell M.J. (2022) Cobalt: a must-have element for life and livelihood. *PNAS*, **119**, e2121307119.

Sasaki S., Prewitt C.T., Sato Y. and Ito E. (1982) Single-crystal X-ray study of gamma-(Mg_2SiO_4). *Journal of Geophysical Research*, **B87**, 7829–7832.

Shannon R.D. (1976) Revised effective ionic radii and systematic study of interatomic distances in halides and chalcogenides. *Acta Crystallographica*, **A32**, 751–767.

Sheldrick G.M. (2015a) SHELXT – Integrated space-group and crystal structure determination. *Acta Crystallographica*, **A71**, 3–8.

Sheldrick G.M. (2015b) Crystal structure refinement with SHELX. *Acta Crystallographica*, **C71**, 3–8.

Solano E., Frontera C., Puig T., Obradors X., Ricart S. and Ros J. (2014) Neutron and X-ray diffraction study of ferrite nanocrystals obtained by microwave-assisted growth. a structural comparison with the thermal synthetic route. *Journal of Applied Crystallography*, **47**, 414–420.

Statista (2021) *Major Countries in Worldwide Cobalt Mine Production in 2021*. Statista Inc, New York, USA [available at www.statista.com/statistics/264928/cobalt-mine-production-by-country/].

Ueno G., Sato S. and Kino Y. (1999) The low-temperature tetragonal phase of $NiCr_2O_4$. *Acta Crystallographica*, **C55**, 1963–1966.

USGS (2022) Cobalt statistics and information. National Minerals Information Center, United States Geological Survey, Virgina, USA [available at www.usgs.gov/centers/nmic/cobalt-statistics-and-information].

Verger L., Dargaud O., Rousse G., Rozsalyi E., Juhin A., Cabaret D., Cotte M., Glatzel P. and Cormier L. (2016) Spectroscopic properties of $Cr^{(3+)}$ in the spinel solid solution $ZnAl_{2-x}Cr_xO_4$. *Physics and Chemistry of Minerals*, **43**, 33–42.

Waerenborgh J.C., Figueiredo M.O., Cabral J.M.P. and Pereira L.C.J. (1994) Temperature and composition dependence of the cation distribution in synthetic $ZnFe_yAl_{2-y}O_4$ ($0<y<1$) spinels. *Journal of Solid State Chemistry*, **111**, 300–309.

Welch, M.D., Cooper, M.A. and Hawthorne, F.C. (2001) The crystal structure of brunogeierite, Fe_2GeO_4 spinel. *Mineralogical Magazine*, **65**, 441–444.

Xiao K.K., Zhang L.L., Tang Q.L., Fan B.B., Hu A.P., Zhang S.Y., Deng W.N. and Chen X.H. (2018) Facile synthesis of single-crystalline Co_3O_4 cubes as high-performance anode for lithium-ion batteries. *Journal of Solid State Electrochemistry*, **22**, 2321–2328.

Yagi T., Marumo F. and Akimoto, S.I. (1974) Crystal structures of spinel polymorphs of Fe_2SiO_4 and Ni_2SiO_4. *American Mineralogist*, **59**, 486–490.

Yamamoto N., Kawano S., Achiwa N. and Higashi S. (1983) Preparation by a wet method and ionic distribution of transition metal-substituted Hausmannite spinel. *Funtai Oyobi Funmatsu Yakin*, **30**, 48–54.

Zhang X., Yang Z., Li C., Xie A. and Shen Y. (2017) A novel porous tubular Co_3O_4: self-assembly and excellent electrochemical performance as anode for lithium-ion batteries. *Applied Surface Science*, **403**, 294–301.

Zhao Z.F. (2016) Study on oxidation rate of orebodies of Sicomines copper-cobalt deposit in D. R. Congo. *China Mining Engineering*, **45**, 1–4 [in Chinese with English abstract].

https://doi.org/10.1180/mgm.2022.27 Published online by Cambridge University Press